Defence Technology 13 (2017) 101–110

Contents lists available at ScienceDirect

Defence Technology

journal homepage: www.elsevier.com/locate/dt

Identifying the optimal HVOF spray parameters to attain minimum porosity and maximum hardness in iron based amorphous metallic coatings

S. Vignesh [a, *], K. Shanmugam [a], V. Balasubramanian [a], K. Sridhar [b]

[a] Centre for Materials Joining and Research (CEMAJOR), Department of Manufacturing Engineering, Annamalai University, Annamalai Nagar 608 002, Tamil Nadu, India
[b] Protective Technologies Department, Naval Materials Research Laboratory (NMRL), Ambernath, Thane (Dist), Maharashtra, India

ARTICLE INFO

Article history:
Received 10 January 2017
Received in revised form
8 February 2017
Available online 4 March 2017

Keywords:
High velocity oxy fuel spray
Iron based amorphous metallic coating
Micro-hardness
Porosity

ABSTRACT

Flow based Erosion – corrosion problems are very common in fluid handling equipments such as propellers, impellers, pumps in warships, submarine. Though there are many coating materials available to combat erosion–corrosion damage in the above components, iron based amorphous coatings are considered to be more effective to combat erosion–corrosion problems. High velocity oxy-fuel (HVOF) spray process is considered to be a better process to coat the iron based amorphous powders. In this investigation, iron based amorphous metallic coating was developed on 316 stainless steel substrate using HVOF spray technique. Empirical relationships were developed to predict the porosity and micro hardness of iron based amorphous coating incorporating HVOF spray parameters such as oxygen flow rate, fuel flow rate, powder feed rate, carrier gas flow rate, and spray distance. Response surface methodology (RSM) was used to identify the optimal HVOF spray parameters to attain coating with minimum porosity and maximum hardness.

1. Introduction

Marine components such as propellers, pumps, impellers experiences erosion-corrosion problems under the solid particle impingement and other flow based environmental conditions. Due to this, every year the ship builders are spending billions of dollars to combat the erosion-corrosion (E-C) degradations [1,2]. Stainless steels are widely used to make many of the marine components because of its capability of resistance to hazardous corrosion, erosion and abrasion damages [3]. Of these, AISI 316L stainless steel provides good E-C resistance under solid particle and slurry based impingement conditions, because of rich content of chromium oxide passive film which resist the surface destructions even in rapid fluid flow and higher temperature conditions (up to 60 °C) [4,5].

Erosion- Corrosion forms on top surfaces and critical sections of the components which are affected by high velocity of fluid flow and slurry impingements. Recently many researchers [6–8] have attempted various coatings on the stainless steel substrate and these coatings include metallic, non metallic and ceramics coatings. Even though organic coatings are cost effective and used in limited applications, they exhibit less resistance to solid particle impingement. Advanced erosion resistance and better binding strength of metallic and ceramics coatings grab more interest in E–C field. It is understood from the literature that ceramics coatings, thermally sprayed WC/Co–Cr and WC coatings are predominantly used for improving E-C resistance.

Recently, a new kind of thermally sprayed iron based amorphous metallic powders (AMCs) were developed with low cost and high hardness [9]. The fabrication of amorphous coatings requires fast cooling rate to prevent formation of nucleation and nucleation growth. Due to this, the microstructure of coating does not contain any crystalline grains and grain boundaries and found to be the sizes of crystallites are in nano scales [10].

One of the ways to achieve the above goal is to employ thermal spraying techniques like high velocity oxy-fuel (HVOF) spray, twin wire arc spraying (TWAS), and atmospheric plasma spraying (APS)

* Corresponding author.
E-mail addresses: vignesh_phd@yahoo.co.in (S. Vignesh), drshanmugam67@gmail.com (K. Shanmugam), visvabalu@yahoo.com (V. Balasubramanian), sridsudi@gmail.com (K. Sridhar).
Peer review under responsibility of China Ordnance Society.

http://dx.doi.org/10.1016/j.dt.2017.03.001

to deposit metallic glass coatings (MGCs). It is evident from the literature [11–13] that the TWAS and APS coatings are resulted in problems such as oxide inclusions, poor interlamellar bonding, high porosity etc. However, HVOF spray process can produce coatings with minimum oxide inclusion, high amorphicity, high hardness and less porosity compared with APS and TWAS processes. It is understood from the literature review that HVOF sprayed iron based amorphous metallic coatings on stainless steel are very scant. Moreover, there is no related information available to predict the porosity and hardness of HVOF sprayed iron based amorphous coatings incorporating HVOF spray parameters. Hence, the current study was undertaken with an objective to develop the empirical relationships to predict the hardness and porosity of HVOF sprayed iron based amorphous metallic coating on naval grade AISI 316 stainless steel substrates. Further, an attempt was also made to optimize the HVOF spray parameters by developing coating with minimum porosity and maximum hardness.

2. Experimental procedure

In this investigation, a commercially available atomized spray quality iron based amorphous powder (Fig. 1) with particle size ranging between −53 and +15 μm (SHS 7574) was used as the coating material. The coating powder was sprayed towards the grit-blasted AISI 316 stainless steel substrate with a surface roughness value of R_a ~ 5 μm. The optical micrograph of the substrate material is shown in Fig. 2. The chemical composition of the substrate material and coating material was found by optical emission spectroscopy method and presented in Table 1.

HVOF (HIPOJET-2700, Make: MEC, India) spraying system was used to develop the iron based amorphous coating to a thickness range of 300–350 μm. The coating thickness was measured by a digital micrometer with an accuracy of 0.001 mm. Standard metallographic procedures were followed to polish the cross-section of the coatings and the average volume percentage of porosity was found. The porosity was measured as per ASTM B 276 on cross-section of the coating (Make: Meiji; Japan, Model: MIL-7100) equipped with an image analyzing software (Metal Vison Version 6). The microhardness of iron based amorphous coatings was recorded using a Vickers micro-hardness tester (Shimadzu, Japan; Model: HMV-2T). A dwell time of 15 s with a load of 300 g was used to measure the hardness. Hardness was measured on the mid thickness of the coating at 15 different locations and the mean value was used for further analysis.

From the past work done in our centre [14], the predominant HVOF spray parameters affecting the coating properties were found, and they are oxygen flow rate, powder feed rate, fuel flow rate, carrier gas flow rate, and spray distance. In this investigation, Design of experiments (DOE) concept was used to minimise

Fig. 1. SEM micrograph of coating material.

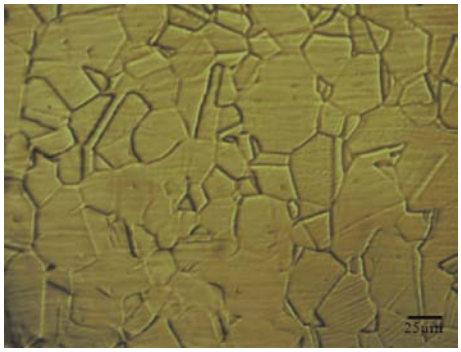

Fig. 2. Light optical micrograph of substrate material.

number of experiments. To identify the feasible working range of HVOF spray parameters, following criteria were adopted. (i) cracks formation and layers separation of the coating, (ii) the formation of coating thickness per pass, (iii) surface roughness must be higher than 5 μm, (iv) with deposition efficiency of 45%–70%, many trial experiments were conducted by varying the HVOF spray parameters and the observations were made during spraying listed below.

(i) If the oxygen flow rate was less than 240 lpm, less fuel was combusted due to lower particle temperature (which is mainly associated with the heat transfer from gas to inflight particles) and resulted in poor melting. If the oxygen flow rate was greater than 260 lpm, fuel was combusted at high melting conditions of inflight particles and resulted in high particle temperature, overheating of the substrate, formation of cracks (due to quenching stress arise during solidification of individual splats since the splats already adhere to the underlying material, tensile stress develop upon cooling and these relax by microcracking).

(ii) If the fuel flow rate was less than 50 lpm, higher porosity in the coating was observed by naked eye. If the fuel flow rate was greater than 70 lpm, bouncing up of unmelted particles was experienced.

(iii) If the spray distance was less than 200 mm, defective microstructure such as pores and splat boundaries were resulted. If the standoff distance was greater than 260 mm, resolidification of molten particles was observed (Table 3).

(iv) If the powder feed rate was less than 24 gpm, only a small amount of powders were injected hence a lesser coating deposition was found. If the powder feed rate was greater than 48 gpm, more unmelted particles, few splats existed in molten state which result in higher porosity (Table 3).

(v) If the carrier gas flow rate was less than 10 lpm, the powder flow was less through the combustion gases. If the carrier gas flow rate was greater than 14 lpm, then the powder moves faster through the combustion gases allowed lower dwell time for the powder, consequently poor melting of the powder was experienced [15]. Based on the above observations, the feasible working range for HVOF spraying was chosen and the values are presented in Table 2.

Table 1
Chemical composition (wt%) of substrate and coating material.

Elements	C	Si	Cr	Ni	Mn	P	Mo	S	Wc	Fe	Bo
Substrate material	0.08	1	18	14	2	0.045	3	0.03	–	Bal	–
Coating material	3	2	25	–	5	–	20	–	10	Bal	5

Table 2
Important HVOF spray parameters and their feasible working range.

No	Factors	Notations	Units	Levels				
				−2	−1	0	1	2
1	Oxygen flow rate	*O*	lpm	240	245	250	255	260
2	LPG flow rate	*L*	lpm	50	55	60	65	70
3	Powder feed rate	*F*	gpm	24	30	36	42	48
4	Spray distance	*S*	mm	200	215	230	245	260
5	Carrier gas flow rate	*C*	lpm	10	11	12	13	14

2.1. Developing the experimental design matrix

Due to the wide range of individual parameters, a central composite rotatable design with five factors and five levels was chosen as an experimental design matrix. Table 4 shows the 32 set of experimental conditions in coded form. The first 16 coded conditions are derived from the half factorial experimental design. The ten star points and six centre points are ensured [16,17]. From the 32 experiments (Table 4), linear (X), quadratic (X^2), and interactive effects (XY) of the variables on the HVOF sprayed iron based amorphous coatings can be evaluated. The higher and lower limits of the factors are assigned as +2 and −2 respectively for the convenience of processing the experimental data. The intermediate coded values can be calculated by using this relationship [17].

$$X_i = 2[2X - (X_{max} + X_{min})]/(X_{max} + X_{min})] \quad (1)$$

Where,

Table 3
Microstructural observation of trial experiments.

Parameter	Level	Microstructural features	Observations
Oxygen flow rate	<240 lpm	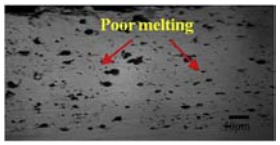	Poor melting
Oxygen flow rate	>260 lpm	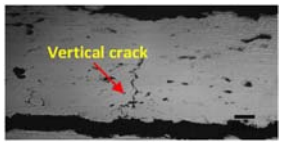	Vertical crack
Fuel flow rate	<50 lpm	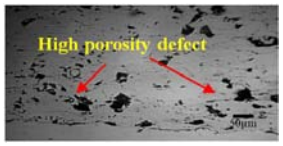	High porosity
Fuel flow rate	>70 lpm	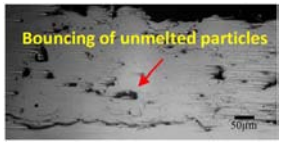	Particles bouncing
Standoff distance	<200 mm	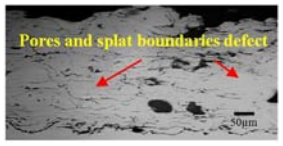	Defect such as pores and splat boundaries
Standoff distance	>260 mm	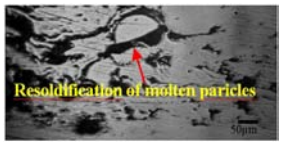	Resoldification of molten particles and porosity
Powder feed rate	<24gpm	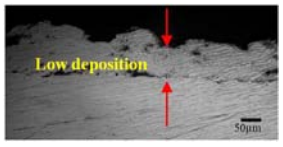	Low deposition
Powder feed rate	>48 gpm	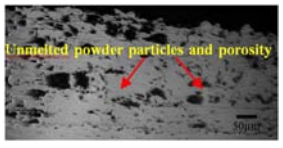	Unmelted fraction and porosity

Table 4
Experimental design matrix and results.

S.no	Coded value						Original value				Responses	
	O	*L*	*F*	*S*	*C*	*O*/lpm	*L*/lpm	*F*/gpm	*S*/mm	*C*/lpm	Porosity/Vol%	Hardness/HV
1	−1	−1	−1	−1	1	245	55	30	215	13	1.93	823
2	1	−1	−1	−1	−1	255	55	30	215	11	0.99	1087
3	−1	1	−1	−1	−1	245	65	30	215	11	1.72	972
4	1	1	−1	−1	1	255	65	30	215	13	0.75	1221
5	−1	−1	1	−1	−1	245	55	42	215	11	1.86	832
6	1	−1	1	−1	1	255	55	42	215	13	1.65	875
7	−1	1	1	−1	1	245	65	42	215	13	0.88	1145
8	1	1	1	−1	−1	255	65	42	215	11	0.75	1210
9	−1	−1	−1	1	−1	245	55	30	245	11	1.5	897
10	1	−1	−1	1	1	255	55	30	245	13	0.45	1288
11	−1	1	−1	1	1	245	65	30	245	13	1.69	873
12	1	1	−1	1	−1	255	65	30	245	11	0.62	1218
13	−1	−1	1	1	1	245	55	42	245	13	2.25	753
14	1	−1	1	1	−1	255	55	42	245	11	2.13	769
15	−1	1	1	1	−1	245	65	42	245	11	2.3	800
16	1	1	1	1	1	255	65	42	245	13	0.9	1041
17	−2	0	0	0	0	240	60	36	230	12	2.22	802
18	2	0	0	0	0	260	60	36	230	12	0.65	1263
19	0	−2	0	0	0	250	50	36	230	12	2.24	794
20	0	2	0	0	0	250	70	36	230	12	1.5	1124
21	0	0	−2	0	0	250	60	24	230	12	0.68	1182
22	0	0	2	0	0	250	60	48	230	12	1.58	892
23	0	0	0	−2	0	250	60	36	200	12	0.95	1074
24	0	0	0	2	0	250	60	36	260	12	1.56	921
25	0	0	0	0	−2	250	60	36	230	10	0.78	1121
26	0	0	0	0	2	250	60	36	230	14	0.6	1200
27	0	0	0	0	0	250	60	36	230	12	0.67	1174
28	0	0	0	0	0	250	60	36	230	12	0.69	1165
29	0	0	0	0	0	250	60	36	230	12	0.7	1150
30	0	0	0	0	0	250	60	36	230	12	0.64	1184
31	0	0	0	0	0	250	60	36	230	12	0.61	1174
32	0	0	0	0	0	250	60	36	230	12	0.73	1156

X_i is the required coded value of variable X and X is any value of the variable from X_{min} to X_{max};
X_{min}- Lower limit of the factor; X_{max}- Higher limit of the factor.

HVOF spraying of iron based amorphous powder on 316 L stainless steel substrate was carried out randomly following the experimental conditions provide by the design matrix to minimize the systematic errors creeping the output responses.

The porosity of the coating was measured following the procedures prescribed by the ASTM B276 standard [18]. The polished cross-section of the coated specimen, comprising an area of about 200 mm^2 was analysed by image analysis software Fig. 3. The porosity was measured at randomly selected three different locations and the average was used for further analysis. The results revealed that the majority of pores present in the HVOF coatings were type A pores (0–10 μm in size). These pores were formed because of interactive effects of particles and the gaseous medium. The microhardness of the coatings was measured at 15 random locations and the average was presented in Table 4. To prevent crack initiation nearby indentations, the indentations distance was kept four times longer than the indentation diagonal. Fig. 4 shows the indentation images on cross section of the coatings.

3. Developing empirical relationships

Coating porosity and coating hardness are the two responses recorded in this investigation. These responses (Y) are the function of HVOF spray parameters such as oxygen flow rate (O), fuel flow rate (L), powder feed rate (F), spray distance (D) and carrier gas flow rate (C). The responses can be expressed as follows

$$Y = f(O, L, F, D, C) \tag{2}$$

The base regression equation chosen to develop empirical relationships to predict porosity and hardness is a portion of a polynomial and it can be expressed as

$$Y = b_0 + \sum b_i x_i + \sum b_{ii} x_i^2 + \sum b_{ij} x_{ixj} \tag{3}$$

and the polynomial equation can be expressed as below by including the effects of main and interaction effects of HVOF spray parameters.

$$\begin{aligned} Y = {} & b_0 + b_1(O) + b_2(L) + b_3(S) + b_4(F) + b_5(C) + b_{12}(OL) \\ & + b_{13}(OS) + b_{14}(OF) + b_{15}(OC) + b_{23}(LS) + b_{24}(LF) \\ & + b_{25}(LC) + b_{11}\left(O^2\right) + b_{22}\left(L^2\right) + b_{33}\left(S^2\right) + b_{44}\left(F^2\right) \\ & + b_{55}\left(C^2\right) \end{aligned} \tag{4}$$

Where b_0 is the average of responses b_1, b_2, b_3, …, b_{55} which are the coefficients depending on respective main and interaction factors [19]. The coefficients were calculated using the Design-Expert software package (version 8.07.1). To identify the significant factors, analysis of variance (ANOVA) test was done and the results are presented in Tables 5 and 6. The final empirical relationships were developed including the significant factors alone and they are given as below

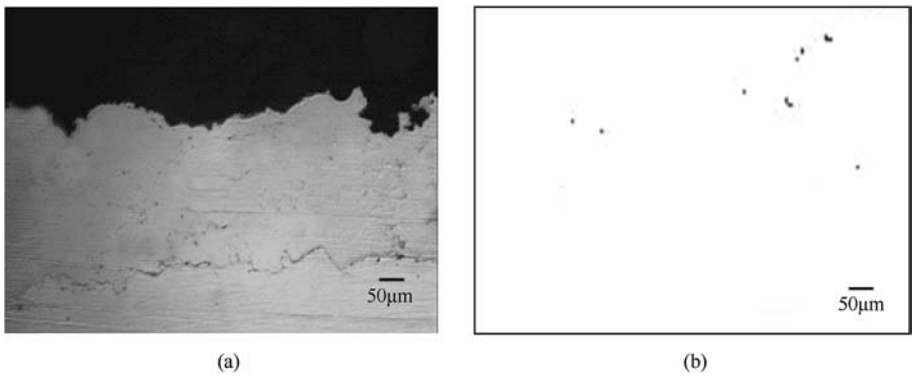

Fig. 3. (a) Optical image selected for porosity analysis, Expt.No.10, (b) binary image for porosity identification.

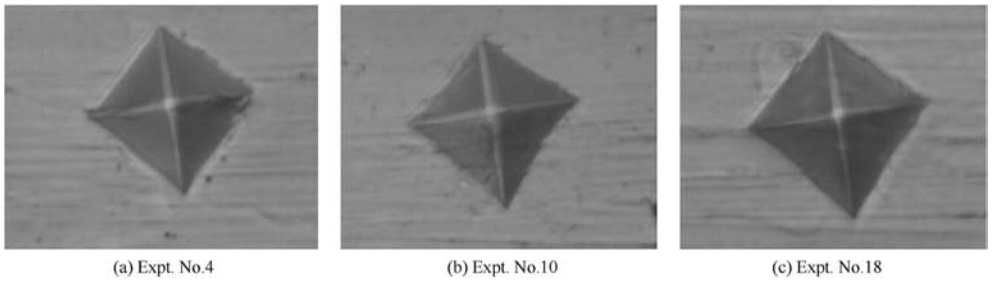

Fig. 4. Micro hardness indentation images.

$$\begin{aligned}\textbf{Coating porosity} = \{&0.68 - 0.38(O) - 0.19(L) + 0.20(F)\\ &+ 0.11(S) - 0.072(C) - 0.078(OL)\\ &+ 0.14(OF) - 0.087(OS) - 0.19(LF)\\ &+ 0.094(LS) - 0.061(LC) + 0.22(FS)\\ &- 0.084(FC) - 0.072(SC) + 0.19\left(O^2\right)\\ &+ 0.29\left(L^2\right) + 0.11\left(F^2\right) + 0.14\left(S^2\right)\ \text{vol.\%}\end{aligned} \tag{5}$$

$$\begin{aligned}\textbf{Coating hardness} = \{&1170.02 + 105.67\,(O) + 75.67(L)\\ &- 63.92(F) - 34.67(S) + 16.33(C)\\ &- 55.25(OF) + 23.25(OS) + 48.62(LF)\\ &- 44.13(LS) - 54.50(FS) + 19.25(SC)\\ &- 36.77\left(O^2\right) - 55.15\left(L^2\right) - 35.65\left(F^2\right)\\ &- 45.52\left(S^2\right)\}HV\end{aligned} \tag{6}$$

From the ANOVA test results, it is found that the value of probability > F and <0.05 for the empirical relationships indicates insignificant factors [20,21]. From the experimentation and prediction results, a relationship has been developed between porosity and hardness as shown in Fig. 5. The data points are fitted by a best fit line. The straight line is governed by the following regression equation:

$$\begin{aligned}&\text{Coating hardness(HV)}\\ &= 1355 - 261(\text{Volume percentage of porosity})\end{aligned} \tag{7}$$

Estimated regression equation (−261) has negative slope, implying that there is an increase in coating hardness with decrease in porosity. The value of coefficient of determination R^2 is 91.80%. It can be interpreted as the percentage of the total sum of squares that can be explained using the estimated regression equation, The goodness of fit of estimated regression equations estimated by coefficient of determination R^2, the fitted regression lines (Eq. (7)) can be used for two purpose;

(a) To determine the mean value of coating hardness for a given value of coating porosity.
(b) To predict the individual value of coating hardness for a given level of coating porosity.

From Fig. 5, it can be suggested that the R^2 value lies between 0 and 1, and this indicates correctness of the developed empirical relationships based on the experimental conditions. Thus, it can be deduced that this R^2 value indicates the good capability of the regression model to predict porosity and hardness.

4. Results and discussion

In this study, porosity and hardness of the as-sprayed coating were chosen as responses for both numerical and graphical optimization. Since the inverse relationship existing between porosity and hardness in thermal spray coatings was well-established [22,23] it is chosen to maximize the hardness and minimize the porosity level to get an optimized condition. The optimized condition was acquired by applying limitations on dependent factors (hardness and porosity) and independent factors (oxygen flow rate, fuel flow rate, powder feed rate, spray distance and carrier gas flow rate). Based on the created regression Eq. (5), coating porosity levels were anticipated and plotted as appeared in Fig. 6(a).

The three dimensional diagrams were plotted against certain

Table 5
ANOVA test results for coating porosity.

Source	Sum of square	*df*	Mean square	*F* Value	Prob > *F*	Source
Model	11.74411	20	0.587205	111.2416	<0.0001	significant
O	3.397538	1	3.397538	643.6376	<0.0001	
L	0.893204	1	0.893204	169.2107	<0.0001	
F	0.988204	1	0.988204	187.2077	<0.0001	
S	0.266704	1	0.266704	50.52507	<0.0001	
C	0.124704	1	0.124704	23.62425	0.0005	
OL	0.097656	1	0.097656	18.50023	0.0013	
OF	0.294306	1	0.294306	55.75407	<0.0001	
OS	0.120756	1	0.120756	22.87635	0.0006	
OC	0.000756	1	0.000756	0.143266	0.7123	
LF	0.551306	1	0.551306	104.4408	<0.0001	
LS	0.142506	1	0.142506	26.99672	0.0003	
LC	0.058806	1	0.058806	11.1404	0.0066	
FS	0.796556	1	0.796556	150.9015	<0.0001	
FC	0.113906	1	0.113906	21.57867	0.0007	
SC	0.082656	1	0.082656	15.6586	0.0022	
O^2	1.006402	1	1.006402	190.6551	<0.0001	
L^2	2.535064	1	2.535064	480.2485	<0.0001	
F^2	0.348364	1	0.348364	65.99491	<0.0001	
S^2	0.576802	1	0.576802	109.2706	<0.0001	
C^2	0.00003	1	0.00003	0.005812	0.9406	
Residual	0.058	11	0.0052			
Lack of fit	0.049	6	0.0081	4.35	0.0640	Not significant
Pure error	0.0093	5	0.0018			
Cor total	11.80	31				
Std. Dev.	0.073	R^2		0.9951		
Mean	1.22	Adj R^2		0.9861		
C.V. %	5.94	Pred R^2		0.8893		
PRESS	1.31	Adeq precision		31.758		

processing conditions to evaluate the effect of process parameters on porosity and hardness. Assist, from the contour plot, it is conceivable to search visually for the best compromise, which remains for the formulation with desirable values for both responses, at the same time. From Fig. 6, it shows that by increasing process parameter such as oxygen flow rate, fuel flow rate, powder feed rate, spray distance and carrier gas flow rate there will be a drop in porosity. The valley of the response graph provides minimum porosity; these response graphs are used to predict the response (porosity) at any region [24–26]. By increasing the flow rate of oxygen, there is a proper combustion of LPG fuel and complete melting of the in-flight particles which leads to good splat formation on the substrate. This results in lower porosity and good bonding strength between the coating and substrate surface [27].

Table 6
ANOVA test results for coating hardness.

Source	Sum of square	*df*	Mean square	*F* Value	Prob > *F*	Source
Model	9.081	20	45406.33	101.6218	<0.0001	significant
O	2.680	1	267970.7	599.7327	<0.0001	
L	1.374	1	137410.7	307.5325	<0.0001	
F	98048.17	1	98048.17	219.4371	<0.0001	
S	28842.7	1	28842.67	64.55144	<0.0001	
C	6402.67	1	6402.667	14.32951	0.0030	
OL	2162.25	1	2162.25	4.839232	0.0501	
OF	48841	1	48841	109.3088	<0.0001	
OS	8649	1	8649	19.35693	0.0011	
OC	144	1	144	0.32228	0.5816	
LF	37830.3	1	37830.25	84.66613	<0.0001	
LS	31152.3	1	31152.25	69.72041	<0.0001	
LC	342.25	1	342.25	0.765974	0.4002	
FS	47524	1	47524	106.3613	<0.0001	
FC	1849	1	1849	4.138161	0.0668	
SC	5929	1	5929	13.26942	0.0039	
O^2	39665.5	1	39665.52	88.77355	<0.0001	
L^2	89210.6	1	89210.64	199.6582	<0.0001	
F^2	37275.6	1	37275.64	83.42488	<0.0001	
S^2	60788	1	60788.02	136.0468	<0.0001	
C^2	668.18	1	668.1818	1.495427	0.2469	
Residual	4914.98	11	446.8168			
Lack of fit	4114.15	6	685.6919	4.281115	0.0660	Not significant
Std. Dev.	21.14	R^2		0.9946		
Mean	1036.88	Adj R^2		09848		
C.V. %	2.04	Pred R^2		0.8834		
PRESS	1.064	Adeq precision		32.304		

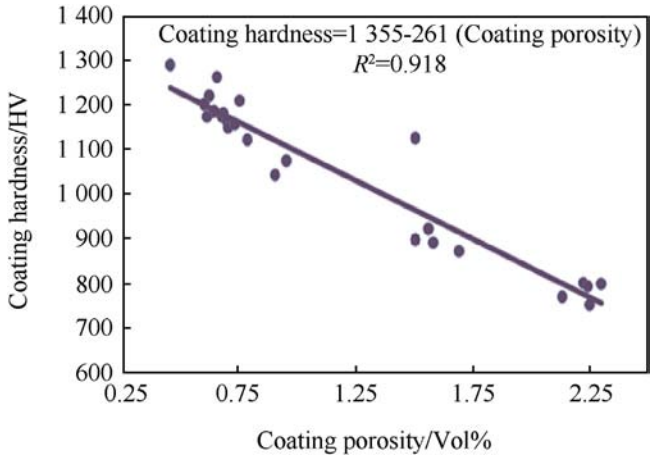

Fig. 5. Relationship between coating porosity and coating hardness.

When the LPG fuel is very low, the flame temperature is also low and it leads to poor melting of coating particles. When the LPG fuel is too high, it leads to oxidation of the coating particles. The oxygen and LPG fuel flow rates are major process parameters and they have an effect on the in-flight particle which inferred the quality of the coating [28].

Moreover, the porosity of the coatings decreased with the oxygen and fuel flow. The higher Oxygen and LPG Fuel flow causes higher particle velocity leads to increased combustion chamber pressure and the spreading of particle and the contact extent will be increased due to the increase in kinetic energy. The porosity can decrease with increase in particle temperature and thus results in denser microstructure [29,30].

Similarly, from the regression Eq. (6), coating hardness was plotted as shown in Fig. 6(b). 3D response surface plots. It is inferred from Fig. 6 that the hardness of coating increases upto a peak level, and then reduces with the increase in the levels of factors. The maximum peak point (apex) of the response graph exhibits the maximum hardness. The effect of powder feed rate (F) is related with spray distance (S) to measure porosity and hardness. From this, powder feed rate (F) is directly proportional to the percentage of porosity and inversely proportional to the hardness. The contour graphs shows that at lower and higher levels of powder feed rate (F) the porosity maximizes and the hardness minimizes due to vaporization of powder and/or improper melting [31,32]. During spraying, the powder feed rate is associated with impact behaviour and heat transfer. By decreasing powder feed rate, very less quantity of coating powder is injected into the chamber as the result high heat energy obtained by the particles which leads to sufficient melting of particles and enhancing good splat formation and it produces low porosity. By increasing powder feed rate, very high quantity of coating powder is injected into the chamber as the result the powder temperature is lower and particles which are large in size get unmelted. recrystallization takes place due to inadequate cooling rate thus porosity of coating increases. The quality of the coatings is good at optimum powder feed rate, in this way most particles are melted [33].

The deposition efficiency can be qualitatively indicated by the coating thickness. The thickness of the coating increases with the increase in the spray distance. The shortest spray distance causes defects in microstructure such as splat boundaries, pores etc. In HVOF spraying, the velocity and temperature of the powder particles will determine the coating characteristics. When particle velocity increases, the kinetic energy of the in-flight particles increases and a raise in particle temperature causes reduction of particle velocity. Both result in reduced splat thickness and produce easy splashing [34,35].

It is observed that, when reducing the spray distance, the porosity increases drastically and decreases the hardness because of kinetic energy variations of in-flight particles. A good suggestion was taken for the intermediate spray distance [31]. Thus, it is

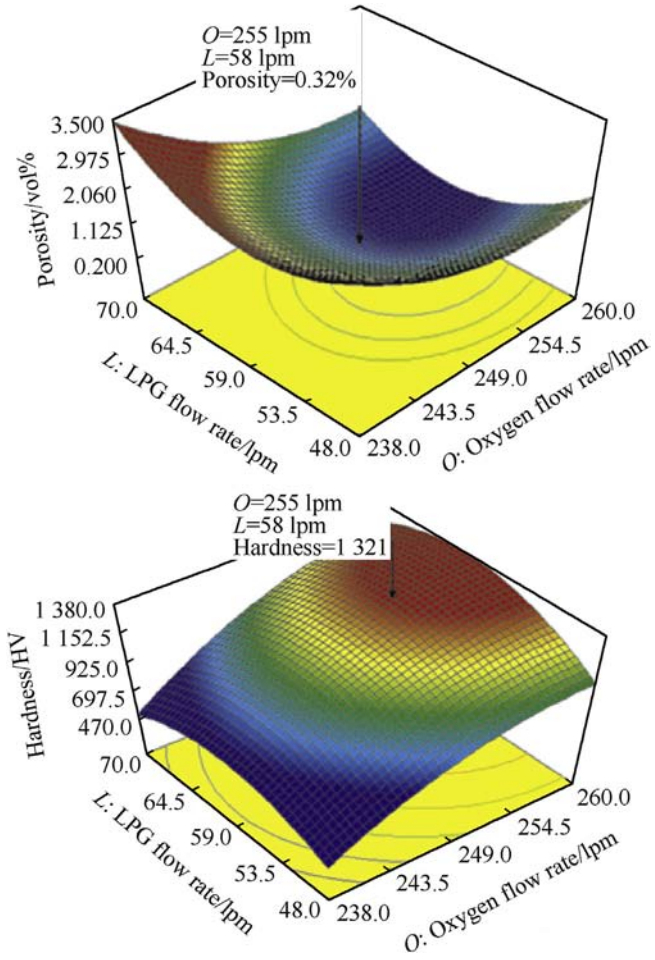

Fig. 6. Response graphs for coating porosity and hardness.

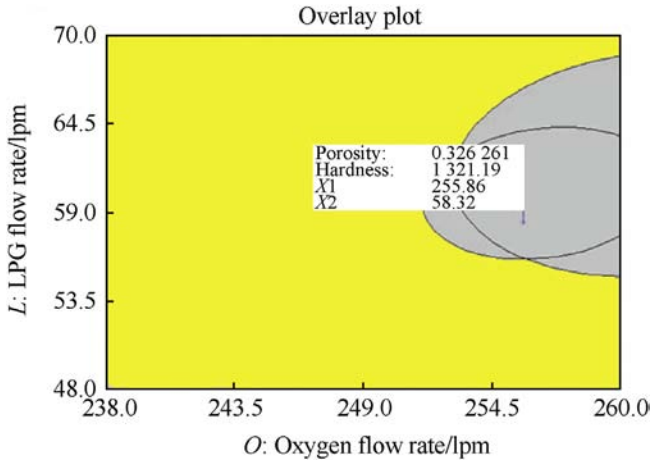

Fig. 7. Overlay plot shows the graphically optimized HVOF spray parameters to attain minimum porosity and maximum hardness.

Table 7
Validation results for developed empirical relationships.

Expt. no.	HVOF spray parameters					Coating porosity/(vol.%)			Coating hardness/(HV 0.3)		
	Oxygen flow rate/lpm	LPG flow rate/lpm	Powder feed rate/(g·min^{-1})	Spray distance/mm	Carrier gas flow rate/lpm	By experiment	By model	Variation/%	By experiment	By model	Variation/%
1	253	63	34	233	12	0.75	0.78	+3.85	1230	1282	+4.05
2	250	64	39	230	13	0.81	0.79	−2.47	1198	1256	+4.62
3	260	66	36	232	14	0.85	0.81	−4.71	1297	1288	−0.7

Table 8
Validation results for optimization procedure.

Expt. no.	HVOF spray parameters					Coating porosity/(vol.%)	Coating hardness/(HV 0.3)
	Oxygen flow rate/lpm	LPG flow rate/lpm	Powder feed rate/(g·min^{-1})	Spray distance/mm	Carrier gas flow rate/lpm		
1	255	58	30	224	12	0.326	1321
2	243	53	31	214	11	2.4	783
3	254	64	42	243	13	2.2	798

important to find a multi-objective maximum strategy where the requirements at the same time meet the desired properties. In this manner, a compromise among the conditions for the two responses to be arrived [36].

With a specific end goal to accomplish such an objective, the multi-objective optimization strategy is utilized. Multiple responses are found from the graphical optimization. In the contour plots, the super imposing or critical response contours are used to identify the feasible regions to attain the proposed criteria. At that point, visual search for the better conciliation becomes possible. On account of managing with many responses, it is recommended to conduct numerical optimization initially; else, one may find it difficult to identify the feasible region. In general, graphical optimization shows the area of feasible regions in the factor space. The regions that are not suitable for the optimization criteria will be shaded [37,38]. The last stage was to overlap the defined desirable areas of both responses to create the region of intrigue or sweet plot. Overlay plots of responses (porosity and hardness) for predicted definitions are outlined in Fig. 7. The light diminishing shade remains for definitions with maximum hardness and minimum porosity.

5. Validation

In the development of empirical relationships, it is critical to figure out if the created relationship predicts the responses accurately. The prediction capability of developed empirical relationships was checked by conducting three more tests utilizing spray process parameters that are not prescribed by the design matrix (Table 4). The experimental and predicted results are presented in Table 7. Predicted values of porosity and hardness derived utilizing developed relationships are in good accordance with the experimental values and the variation is observed to be within ±5%. From the above results, it is confirmed that the established relationships can be viably applied to predict hardness and porosity of HVOF sprayed iron based iron based amorphous coatings at 95% confidence level.

To affirm the outcomes got through numerical modelling (suggested solutions), the HVOF tests were led with the spray parameters recommended by the model, to be specific, keeping the oxygen flow rate, fuel flow rate, carrier gas flow rate, spray distance and powder feed rate at 255 lpm, 58 lpm, 12 lpm, 227 mm and 30 g/min respectively. Further, extra two set of investigations were conducted above and below the optimized spraying conditions and the observed results are presented in Table 8. From these outcomes, it is observed that varying spray parameters from the optimized conditions prompts to the increase in coating

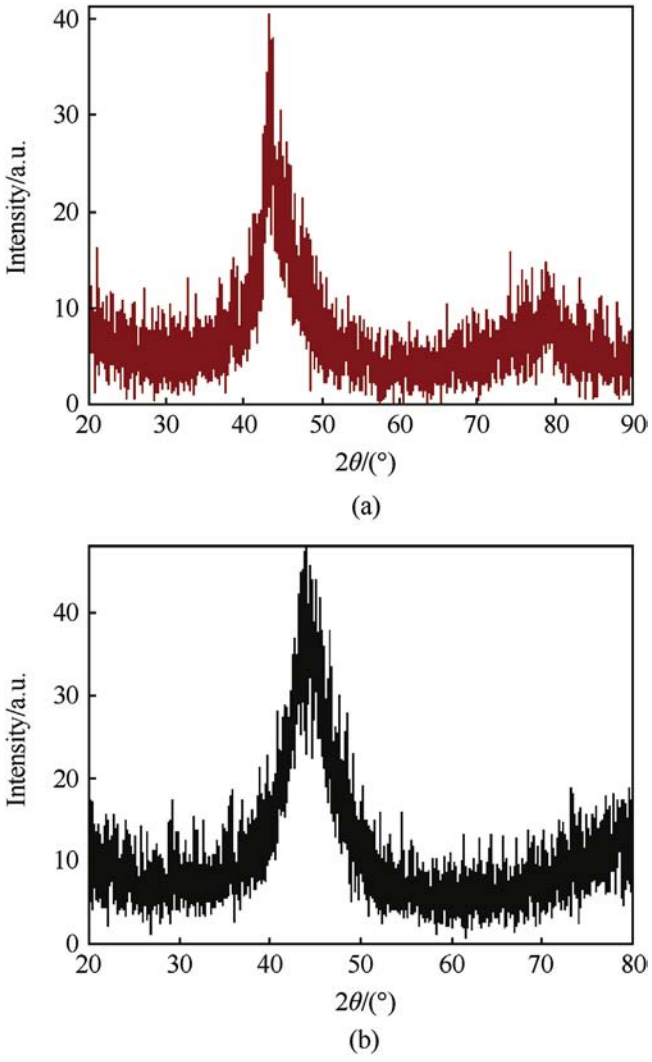

Fig. 8. XRD pattern analysis of (a) Powder and (b) Coating.

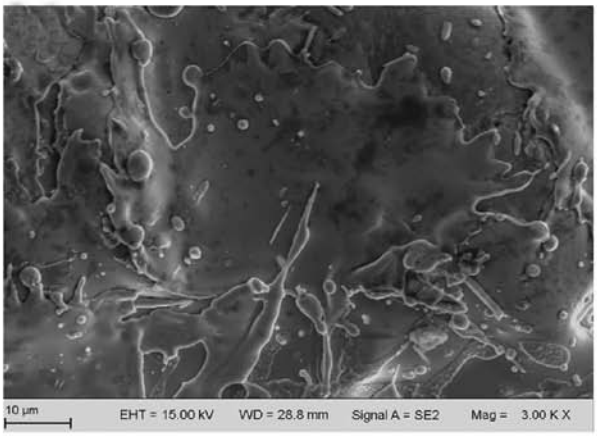

(a)

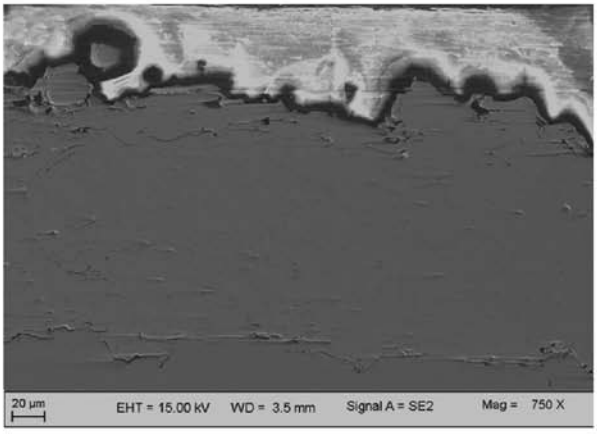

(b)

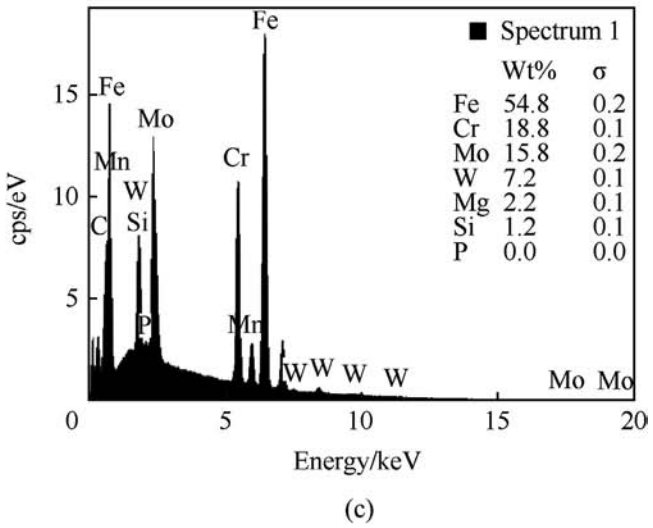

(c)

Fig. 9. SEM micrograph of coating deposited using optimized HVOF spray condition. (a) Coating top surface, (b) coating cross section, (c) EDS analysis of coating top surface.

porosity and decrease in coating hardness, This is because of enthalpy provided from the flame to the powder particles, differences in dwell time of the particles in the flame and variations in spray distance.

The iron based amorphous powder and as-sprayed coatings was examined by XRD and presented in Fig. 8. XRD patterns shows a broad diffraction hump at 2 θ = 40-50° without any Bragg peaks. From the characterization of powder and coating materials, that exhibits a broad diffraction hump without any refraction from crystal phases indicating that the coating is amorphous. Similar results were reported in past works [39–41]. HVOF coating have superior surface finish compared with other thermal spray process and the microstructure reveals the plastic deformation of unmelted particles results in rapid solidification of droplets upon substrate impingement. The optimized process parameter and appropriate particle size of powder will lead to proper melting of in flight particles to achieve efficient surface splat formation of coating on the substrate. Since the coating deposited at an optimized process condition has exhibited less porosity and high hardness of iron based amorphous coating as seen in Fig. 9.

6. Conclusions

1) Statistical tools such as design of experiments (DoE) and Analysis of Variance (ANOVA) have been successfully employed to identify the most relevant factors influencing the HVOF spraying of amorphous powders. The oxygen flow rate could be identified as the most significant influencing factor with respect to the porosity and hardness of the coating.
2) Using response graphs and contour plots, optimum spray settings was identified, They are: oxygen flow rate of 255 lpm, fuel flow rate of 58 lpm, spray distance of 224 mm, powder feed rate of 30 g/min and carrier gas flow rate 12 lpm,
3) Coatings sprayed with optimized process parameter and appropriate particle size of powder led to proper melting of in flight particles to achieve efficient surface splat formation of coating on the substrate. Hence, the coating deposited at an optimized process condition has exhibited less porosity and high hardness of iron based amorphous coating.
4) Verification experiments yielded mostly excellent results in close proximity to the predicted values. The deposited fine structured amorphous coatings showed an extremely dense coating structure with porosity (0.32 vol.%) and hardness (1321HV).

These coatings show a high potential to be used as erosion corrosion resistance for marine application.

Acknowledgments

The authors wish to express their sincere thanks to The Director, Naval Materials Research Laboratory (NMRL), Ambernath, Maharastra for providing the coating materials to carry out this investigation.

References

[1] Wood RJK, Speyer AJ. Erosion–corrosion of candidate HVOF aluminium-based marine coatings. Wear 2003;256:545–56.
[2] Lakshminarayanan AK, Ramachandran CS, Balasubramanian V. Feasibility of surface- coated friction stir welding tools to join AISI 304grade austenitic stainless steel. Def Tech 2014;10:360–70.
[3] Fang Luo, Andrew Cockburn, Martin Sparkes, Rocco Lupoi, Zhi-jun Chen, William O'neill, Jianhua Yao, Rong Liu. Performance characterization of Ni60-WC coating on steel processed with supersonic laser deposition. Def Tech 2015;11:35–47.
[4] Wang Y, Xing ZZ, Luo Q, Rahman A, Jiao J, Qu SJ, Zheng YG, Shen J. Corrosion and erosion–corrosion behaviour of activated combustion high-velocity air fuel sprayed Fe-based amorphous coatings in chloride-containing solutions. Corros Sci 2015;98:339–53.
[5] Zhou H, Zhang C, Wang W, Yasir M, Liu L. Microstructure and mechanical properties of Fe-based amorphous composite coatings reinforced by stainless steel powders. J Mater. Sci Technol 2015;31:43–7.
[6] Sasaki K, Burstein GT. Erosion Corrosion of stainless steel under impingement by a fluid jet. Corros Sci 2007;49:92–102.

[7] Wang YG, Zheng YG, Ke W, Sun WH, Hou WL, Chag XC, Wang JQ. Slurry erosion–corrosion behaviour of high-velocity oxy-fuel (HVOF) sprayed Fe-based amorphous metallic coatings for marine pump in sand-containing NaCl solutions. Corros Sci 2011;53:3177–85.
[8] Burstein GT, Sasaki K. Effect of impact angle on the slurry erosion corrosion of 304L stainless steel. Wear 2000;240:80–94.
[9] Rajahram SS, Harvey TJ, Wood RJK. Erosion Corrosion resistance of engineering materials in various test conditions. Wear 2009;267:244–54.
[10] Hu X, Neville A. The electrochemical response of stainless steels in liquid-solid impingement. Wear 2005;258:641–8.
[11] Wang Y, L Jiang S, Zheng YG, Ke W, Sun WH, Wang JQ. Effect of porosity sealing treatments on the corrosion resistance of high-velocity oxy-fuel (HVOF)-sprayed Fe- based amorphous metallic coatings. Surf Coat Technol 2011;206:1307–18.
[12] Cherigui M, Feraoun HI, Feninehe* NE, Aourag H, Coddet C. Structure of amorphous iron-based coatings processed by HVOF and APS thermally spraying. Mater. Chem Phys 2004;85:113–9.
[13] BavarescoSucharski Gustavo, Pukasiewicz Anderson Geraldo Marenda, Váz Rodolpho Fernando, Paredes Ramón Sigifredo Cortés. Optimization of the deposition parameters of HVOF FeMnCrSi+Ni+B thermally sprayed coatings. Soldagem Inspeção 2015;20(2):238–52.
[14] Murugan K, Ragupathy A, Balasubramanian V, Sridhar K. Optimizing HVOF Spray Parameters to attain minimum porosity and maximum hardness in WC-10Co-4Cr Coatings. Surf Coat Technol 2014;247:90–102.
[15] Thiruvikraman C, Balasubramanian V, Sridhar K. Optimizing HVOF spray parameters to maximize bonding strength of WC-CrC-Ni coatings on AISI 304L stainless steel. ASM Int 2014;23:860–75.
[16] Doring E, Vaben R, Stover D, Julich D. The influence of spray parameters on particle properties. In: ITSC-international thermal spray conf (DVS-ASM); 2002. p. 440–8. Paper 3.
[17] Miller RG, Freund JE, Johnson DE. Probability and statistics for engineers. New Delhi: Prentice of Hall of India Pvt. Ltd.; 1999.
[18] Thirumalaikumarasamy D, Shanmugam K, Balasubramanian V. Establishing empirical relationships to predict porosity level and corrosion rate of atmospheric plasma-sprayed alumina coatings on AZ31B magnesium alloy. J Mater. Process Technol 2014;2:140–53.
[19] Montgomery DC. Design and analysis of experiments. 2nd ed. New York: Wiley; 1984.
[20] Mugadeeswaran G, Sreehari R Nair, Sundarb L, Harikannan N. Optimization of process parameters of the activated tungsten inert gas welding for aspect ratio of UNS S32205 duplex stainless steel welds. J. Defence Tech 2014;10:251–60.
[21] Thirumalaikumarasamy D, Shanmugam K, Balasubramanian V. Developing empirical relationships to predict porosity and microhardness of atmospheric plasma sprayed alumina coatings on AZ31B magnesium alloy. J Manuf Sci Prod 2015;15:169–81.
[22] Cho JY, Zhang SH, Cho TY, Yoon JH, Joo YK, Hur SK. The processing optimization and property evaluations of HVOF Co-base alloy T800 coating. J Mater. Sci 2009;44:6348–55.
[23] Tillmann W, Vogli E, Baumann I, Kopp G, Weihs C. Desirability-based multicriteria optimization of HVOF spray experiments to manufacture fine structured wear- resistant 75Cr3C2-25(NiCr20) coatings. J Therm Spray Technol 2010;19:392–408.
[24] Kaur M, Singh H. A survey of the literature on the use of high velocity oxy-fuel sprays technology for high temperature corrosion and erosion–corrosion resistant coatings. Anti Corros. M 2008;55(2):86–96.
[25] Zhou Z, Wang L, Wang FC, Zhang HF, Liu YB, Xu SH. Formation and corrosion behavior of Fe-based amorphous metallic coatings by HVOF thermal spraying. Surf Coat Technol 2009;204:563–70.
[26] Kawakita J, Kuroda S, Kodama T. Evaluation of through-porosity of HVOF sprayed coating. Surf Coat Technol 2003;166:17–23.
[27] Dongmo E, Wenzelburger M, Gadow M. Analysis and optimization of the HVOF process by combined experimental and numerical approaches. Surf Coat Technol 2008;202:4470–8.
[28] Bansal P, Shipway PH, Leen SB. Residual stresses in high-velocity oxy-fuel thermally sprayed coatings-Modelling the effect of particle velocity and temperature during the spraying process. Acta Mater 2007;55:5089–101.
[29] Mostaghimi J, Chandra S, Ghafouri-Azar R, Dolatabadi A. Modelling thermal spray coating processes: a powerful tool in design and optimization. Surf Coat Technol 2003:163–4.
[30] Turunen E, Varis T, Gustafsson TE, Keskinen J, Fält T, Hannula SP. Parameters optimization of HVOF sprayed nanostructured alumina and alumina-nickel composite coatings. Surf Coat Technol 2006;200:4987–94.
[31] Zhang W, Sampath SA. Universal method for representation of in-flight particle characteristics in thermal spray processes. J Therm Spray Technol 2009;18:23–34.
[32] Verdon C, Karimi A, Martin JL. A study of high velocity oxy-fuel thermally sprayed tungsten carbide based coatings. Part 1: Microstructures. Mater. Sci Eng A 1998;246:11–24.
[33] Liu Lin, Zhang Cheng. Fe-based amorphous coatings: structures and properties. Thin Solid Films 2014;561:70–86.
[34] Berget J, Rogne T, Bardal E. Erosion-corrosion properties of different WC-Co-Cr coatings deposited by the HVOF process-Influence of metallic matrix composition and spray powder size distribution. Surf Coat Technol 2007;201:7619–25.
[35] Lima RS, Marple BR. From APS to HVOF spraying of conventional and nanostructured titania feedstock powders: a study on the enhancement of the mechanical properties. Surf Coat. Technol 2006;200:3428–37.
[36] Dwivedi G, Wentz T, Sampath S, Nakamura T. Assessing process and coating reliability through monitoring of process and design relevant coating properties. J Therm Spray Technol 2010;19:695–712.
[37] Balasubramanian V, Lakshminarayanan AK, Varahamoorthy R, Babu S. Understanding the parameters controlling plasma transferred arc hardfacing using response surface methodology. Mater. Manuf Proc 2008;23:674–82.
[38] Jarrah NA. Studying the influence of process parameters on the catalytic carbon Nano fibers formation using factorial design. J Chem Eng 2009;561:367–71.
[39] Cheng Y, Ma E. Atomic-level structure and structure–property relationship in metallic glasses. Prog Mater. Sci 2011;56(4):379–473.
[40] Trexler MM, Thadhani NN. Mechanical properties of bulk metallic glasses. Prog Mater. Sci 2010;55(8):759–839.
[41] Zhang T, Liu T, Pang S, Li R. Ductile Fe-based bulk metallic glass with good soft magnetic properties. Mater. Trans 2007;48(5):1157.